Release of content through mechano-sensitive gates in pressurized liposomes

Louhivuori, Martti; Risselada, Herre; Giessen, Erik van der; Marrink, Siewert J.

Published in:
Proceedings of the National Academy of Sciences of the United States of America

DOI:
10.1073/pnas.1001316107

Publication date:
2010

Supporting Information

Louhivuori et al. 10.1073/pnas.1001316107

SI Materials and Methods

System Setup. Molecular dynamics simulations of MscL in model liposomes were carried out using a modified version (1) of GROMACS (2) with mean-field force approximation (MFFA) boundary potentials. The MFFA boundary potential is an effective potential that mimics the bulk water surrounding the liposome (1). This procedure has the computational advantage that most of the external water can be removed without any adverse effect on the properties of the liposome.

The MARTINI coarse-grained force field (3) was used in conjunction with its recently released extension (4) for protein models. A MARTINI CG protein model has a static, predefined secondary structure but is able to undergo even large-scale changes in its tertiary structure. The standard simulation protocol associated with the MARTINI force field was used, i.e., shifted (5) Coulombic and van der Waals potentials with a cutoff of 1.2 nm. All the simulations were run with a 20-fs time step, and the system was coupled to a Berendsen thermostat (6) maintaining a temperature of 310 K. The system was enveloped in a pressure bath of 1 bar via coupling of the external MFFA potential (1).

The initial system was obtained by immersing the crystal structure of Tb-MscL in its closed state (7) in a spontaneously formed lipid vesicle followed by equilibration of the system. The approximately 16-nm diameter liposome contained 2,108 DOPC lipids and 5,444 water beads with an additional 54,649 water beads forming an approximately 4-nm water layer around the vesicle. Note that each coarse-grained water bead actually represents four real water molecules. The complete system was surrounded by an MFFA boundary potential with a diameter of approximately 28.5 nm.

Increasing Internal Pressure. MscL activation was triggered by gradually increasing the internal pressure of the liposome. This was achieved by having an additional MFFA potential in the center of the liposome that acted as a water piston capable of creating a water-fillable cavity inside the vesicle. Once created, this cavity was filled with water and the process was repeated in a number of pumping cycles. In the beginning of each pumping cycle the internal MFFA potential had a radius of 0.1 nm, which was slowly increased during an 80-ns simulation to the maximum of 3.9 nm. At this point the cavity was filled with 2,142 water beads, the radius of the internal MFFA potential was reset, and a new pumping cycle was started. The internal MFFA potential was completely removed prior to the steady-state simulations started after each of the nth pumping cycle. Simulations at these intermediate stages, for which the MscL channel remained closed, were performed for up to 4,000 ns. The exact system compositions and details of the intermediate stages can be found in Table S1. System VI was the first one to have an open channel and is the initial structure for the extensive simulations of 40 μs presented in the main article. Note that the sampling times indicated here, and in the main manuscript, are effective times, four times longer than the actual simulation time; this scaling factor accounts for the increase in the speed of dynamics in coarse-grained simulations due to a smoothened energy landscape (3).

Additional simulations were also performed, e.g., using a higher loading rate, i.e., 660 kN/m·s compared to 140 kN/m·s. This resulted in a partial activation of the channel (subconducting state) followed by membrane rupture (Fig. S2). Similar simulations of pure lipid vesicles without MscL (Fig. S1) show comparable rupture strength and confirm that the protein channel requires sufficient reaction time to successfully activate prior to membrane rupture. As a control, the channel activation was also repeated 10 times using different starting points from the steady-state simulation V with gating observed in six of the cases. In those cases where gating was observed, results were similar to those reported in the main article.

Water-Repellent Lipid Tails. In order to impose high enough surface tension in the membrane for MscL activation, the model liposomes need to have a relatively high internal pressure (exceeding 100 bar). The problem with this is that, quite realistically, a model liposome does not sustain such a high pressure gradient for a long time. Water will leak through the membrane at a rate that is, from a technical point-of-view, too quick. If left unchecked it would render the above-described water-piston method useless, because all the waters displaced by the internal MFFA potential would simply push other waters through the membrane already during the 80-ns pumping run. Thus, we have made a small modification to the lipid tails that almost completely prevents water flux through the membrane without affecting other thermodynamic properties of the liposome. A water-repellent lipid is a completely normal lipid in all other ways except for the lipid–water interactions of the last bead of the lipid tails (Fig. S5). The modified, water-repellent C5 bead is called wC5 and has a slightly longer-ranged repulsive interaction with P4 beads (i.e., water). The width σ of the Lennard-Jones potential

$$U(r) = 4\varepsilon\left[\left(\frac{\sigma}{r}\right)^{12} - \left(\frac{\sigma}{r}\right)^{6}\right] \qquad \text{[S1]}$$

is increased, i.e., $\sigma = 0.47 \rightarrow 0.70$, while the depth ε of the potential well is kept the same. This means that water beads feel an excluded volume barrier in the bilayer center (where most of the tail terminal groups reside), blocking them from permeating across the membrane. The effects of this modification on other membrane properties are negligible (Table S2). For example, at 310 K the bilayer thickness of both DOPC and wDOPC bilayers is (4.52 ± 0.03) nm and the area per lipid is (68.5 ± 0.2) Å^2 and (68.4 ± 0.3) Å^2, respectively—well within the margins of error.

Lateral Tension and Pressure. The analysis of 3D pressure fields inside the system was done as a postsimulation trajectory analysis using a method we have developed (8) recently. The whole system is first divided into small, $0.4 \times 0.4 \times 0.4$ nm^3 volume elements, i.e., voxels. The local pressure field is then calculated for each voxel over the desired time interval. Because a liposome system is spherically symmetric, one can then proceed to calculate, e.g., an average pressure profile as a function of distance from the liposome center. The internal pressure, and thus also the pressure difference across the membrane, can be directly calculated from the 3D pressure field. Note that the external pressure is kept at 1 bar by a barostat. The reported internal pressures are calculated as the average of the three Cartesian components obtained by a normalized, cumulative sum over all voxels inside the liposome, and the error estimate is the standard deviation of the three components from the average.

The surface of a spherical liquid droplet immersed in another liquid with a lower hydrostatic pressure experiences a lateral stress, i.e., surface tension, which is proportional to the pressure difference between the two liquid phases. According to the Laplace equation (9) this relation is given as

$$\Delta P = \frac{2\gamma}{r}, \qquad \textbf{[S2]}$$

where ΔP is the pressure difference, γ the surface tension, and r the radius of the droplet. In this study Eq. **S2** is used to estimate the surface tension in a liposome from the known pressure difference and radius of the liposome.

Conversely, the lateral stress in a liposome can also be calculated directly from the local 3D pressure fields by averaging over the spherical symmetry. From the radially averaged normal P_N and tangential P_T pressure components one can calculate the average hydrostatic pressure

$$p(r) = (P_N(r) + 2P_T(r))/3 \qquad \textbf{[S3]}$$

as well as the average pressure differential, or pressure profile as it is often called,

$$\tau(r) = P_N(r) - P_T(r). \qquad \textbf{[S4]}$$

The surface tension at the surface of tension r_s is then the normalized integral (9) of the pressure differential over the membrane region, i.e.,

$$\gamma = r_s^{-2} \int_0^\infty r^2 \tau(r). \qquad \textbf{[S5]}$$

The pressure profiles and the hydrostatic pressures for the first 400 ns of systems I and VI are shown in Fig. S6. Assuming an equimolar surface of tension, Eq. **S5** gives a surface tension of 27 mN/m and 67 mN/m for the two liposomes, respectively. The higher surface tension (system VI) is, within the margin of error, equal to the one given by Eq. **S2** (Table S1), while the lower surface tension (system I) is slightly higher than the Laplace tension. This is not unexpected, as it is known (10) that the actual surface of tension can greatly deviate from the equimolar surface for a lipid membrane under low surface tension.

Relaxation of Liposomal Stress. In order to estimate the time it would take for the liposome to reach a tensionless state and a zero pressure difference, the linear regions (8–40 μs) of surface tension and pressure curves were fitted to linear decay functions. From these one finds that it would take at least (86 ± 4) μs to have no surface tension in the membrane and (93 ± 4) μs to fully equalize the pressure inside and outside of the liposome (Fig. S4).

SI Results

Response of Liposomes. A liposome stressed beyond its elastic limits and without any means to alleviate the stress has only a limited lifetime before it undergoes lysis. The expected lifetime depends on the amount of stress on the membrane, i.e., on the pressure difference across the membrane. Once nucleation has occurred, a membrane pore grows rapidly and allows for the internal and external solvents to equalize, thus relaxing the stress on the liposome. In some cases this is followed by a slow shrinking and subsequent closure of the pore (Fig. S1).

At a sub-microsecond loading rate (140 kN/m·s), we observe the vesicular membrane of a pure lipid vesicle to rupture at an estimated membrane tension of (69 ± 1) mN/m, similar to the surface tension required for channel activation. The rupture tension is about six times larger than observed (11) experimentally. This can be attributed to the difference in time scale, combined with a size effect as larger vesicles have simply more membrane surface available for rupture.

As we have shown, MscL provides an efficient way to alleviate the stress due to an osmotic shock, provided there is enough reaction time to activate before membrane rupture. When a too-high loading rate is used (660 kN/m·s), sufficient reaction time is denied leading to a membrane rupture instead of channel activation (Fig. S2). In other words, the probability of membrane rupture within a certain time window is much higher than the probability of channel activation.

Gating Mechanism. It has been suggested (12) that the activation of MscL involves an iris-like opening of the channel in conjunction with the dissociation of the cytoplasmic bundle. The transmembrane helices would slide anticlockwise (seen from the periplasmic side) increasing their tilt from the channel normal, thus creating a large pore through the membrane. After dissociation the cytoplasmic helices would line the rim of the channel so as to further stabilize it. The iris-like opening has been confirmed to be a viable model for MscL activation by multiple computational and experimental studies (13–15), but the role of the cytoplasmic helix-bundle has been a topic of much speculation (16, 12, 17). We further confirm that the opening of MscL does not require the dissociation of the helix bundle and, vice versa, that the dissociation of the helix-bundle does not per se render the channel nonfunctional.

The observed mechanism of MscL opening follows roughly the proposed (12) iris-like model with the transmembrane helices reorienting more loosely and at a more pronounced angle from the membrane normal. Contrary to the beautiful, fivefold symmetric opening—forced, e.g., by Jeon and Voth in a steered-MD study (18)—the free, nonbiased MscL seems to open in a distinctly asymmetric manner (Fig. S3). The transmembrane helices tilt simultaneously, but independently, to accommodate the thinning of the membrane. The tilt angles of the transmembrane helices TM1 and TM2 relative to the channel direction change from $(38.3 \pm 0.1)°$ and $(21.9 \pm 0.4)°$ in the closed state to $(76.0 \pm 0.1)°$ and $(56.1 \pm 0.1)°$ in the open state, respectively. While tilting, TM1 and TM2 also move away from the channel center to form a larger ring-like lining of the enlarged membrane pore. The surface area of the open channel (60 nm^2, including both protein and channel) is more than two times larger than that of the closed channel (26 nm^2). N-terminal helices follow the movement of TM1 staying parallel to the membrane surface but do not show any indication of either moving to block the channel or to line the rim of the channel as has been suggested (12).

As shown (19) by Elmore and Dougherty the C-terminal helix bundle of the first crystal structure (1MSL) was unstable at physiological conditions, unlike in the revised crystal structure (2OAR, used also in this study) as shown (20) recently by Maurer et al. Indeed, we do not see any twisting of the helices that would bury the nonpolar residues within the bundle and expose more polar residues to the solvent nor do we see the suggested expansion of the bundle due to repulsion between acidic groups in pH 7. Immediately after activation the bundle of C-terminal helices is intact and pushed slightly away from the mouth of the channel. After 20 μs the C-terminal helices have partly dissociated and reoriented along the rim on one side of the channel. From time to time few helices enter inside the channel and partially block the flow through the channel.

The role and dynamics of the C-terminal helix bundle has been the subject of much discussion (16, 12, 17). Initially, Sukharev et al. postulated (12) that the dissociated C-terminal helices might compensate for the thinning of the membrane by interacting with the cytoplasmic lipids, but later they retracted (16) this, reporting that there was no evidence of dissociation in MD simulations of the C-terminal domain. However, in our simulation we do observe a partial dissociation of the helix-bundle after a lengthy postactivation time period, as shown in Fig. S3 after 20 μs of simulation. The transmembrane helices pull, through the linkers, the nonterminal ends of the helical bundle apart from each other, giving the bundle a cone-like shape as seen for the

open channel in Fig. S3. Even though the constant pulling facilitates the dissociation of the helices, it seems that complete breakage of the bundle requires a considerable amount of energy making it thermodynamically unlikely. When the bundle finally dissociates the helices are still clinging to each other, suggesting that it would take considerably longer than 40 μs for them to assume symmetrical positions around the ring.

Our findings point to a possible different role of the C-terminal helix bundle, pertaining to the mechanism of closure of the channel. The partial dissociation of the C-terminal helix bundle allows the helices to intermittently enter the channel and to obstruct the free flow of solvent. This occurs after 20 μs of simulation (Fig. S3). We speculate that, by blocking the flux through the channel, the helices may give MscL an opportunity to constrict once again without the need of dewetting the channel first. During the last 20 μs of the simulated 40 μs the blocking was seen to occur multiple times, although a permanent in-activation of MscL was not observed.

Control Simulations

In order to satisfy that the coarse-grained model used in the study is indeed valid for the simulated process, we have done some additional control simulations to test the sequence specificity and sensitivity of the model channel. It has already been shown (14) that a MARTINI CG model of MscL is sensitive to a point mutation in the pore region, i.e., gain-of-function mutant V21D was shown to lower the gating threshold significantly in agreement with experimental measurements (21).

We have looked into three separate alterations of the MscL structure: (*i*) cleaving off of the extramembrane loops and helices, and (*ii*) in addition changing all residues to alanines, or (*iii*) replacing the transmembrane helices with WALP peptides (22). All simulations were started from a preequilibrated system consisting of a closed MscL channel embedded in a 17×17 nm lamellar bilayer of 504 DOPC lipids and surrounded by an approximately 5-nm water layer on either side. Eight independent 480-ns simulations were done for each system. Identical conditions and parameters were used as in the main study.

Deletion Mutants. It has been experimentally shown (23, 24) that, on one hand, the cleaving of extramembrane loops and/or helices from an *E. coli*-MscL can adversely effect the channel's ability to function but, on the other hand, large segments from either N terminus or C terminus can be safely cleaved without any adverse effects. Removal of either the periplasmic linkers or the complete cytoplasmic domain results in a total loss of mechano-sensitive activity. It is not known what exactly causes the loss of functionality, but it has been speculated (23) that at least the loop regions are essential for either the channel activation or the correct folding/assembly of the protein.

We have simulated both the Δ103 mutant (no cytoplasmic helices) as well as the Δ12-Δ47/68-Δ101 triple mutant (everything but TM1 & TM2 removed) of Tb-MscL [correspond to Δ110 and NBE-ΔEV-Δ104 of E.Coli-MscL, respectively (23)]. In agreement with experiments, Δ103 is mechano-sensitive and similarly to the wild-type MscL activated in three out of the total eight trial simulations.

Seemingly contrary to experiments, the Δ12-Δ47/68-Δ101 triple mutant is also mechano-sensitive and activates even with a slightly increased likelihood (6/8 v. 3/8). This suggests that either mis-folding or a disturbed subunit assembly is the cause of the measured inactivity of the NBE-ΔEV and Δ104 E.Coli-MscL mutants (23).

See Table S3 for a comparison of the activation likelihood of each of the tested mutants to those of the wild-type MscL and the gain-of-function mutant V21D (14).

Sequence Specificity. Because the Δ12-Δ47/68-Δ101 triple mutant was shown to be mechano-sensitive and capable of forming a functional membrane channel, it was chosen as the most simplified base model for looking at the sequence specificity of MscL.

First, the transmembrane helices TM1 and TM2 were changed to polyalanines. Not only was the resulting "channel" incapable of activation it also served as an impurity in the membrane that lead to the nucleation of a membrane pore after 460 ns (Fig. S7).

Second, to make sure that the loss of mechano-sensation is not limited to only the extreme case of a polyalanine, we also took the transmembrane helices TM1 and TM2 and changed their amino acid sequence to that of a WALP peptide (22), i.e., WWALAL… ALALWW. In all of the simulations, the channel remained inactive and no membrane poration was observed. Because the expected lifetime of a DOPC membrane under a 65 mN/m tension is in the microsecond time scale, it can be safely concluded that the transition of TM1 and TM2 to WALP peptides renders the channel insensitive to mechanical stress without increasing the likelihood of membrane rupture.

1. Risselada HJ, Mark AE, Marrink SJ (2008) Application of mean field boundary potentials in simulations of vesicles. *J Phys Chem B* 112:7438–7447.
2. Hess B, Kutzner C, van der Spoel D, Lindahl E (2008) GROMACS 4: Algorithms for highly efficient, load-balanced, and scalable molecular simulation. *J Chem Theory Comput* 4:435–447.
3. Marrink SJ, Risselada HJ, Yefimov S, de Vries AH (2007) The MARTINI force field: Coarse grained model for biomolecular simulations. *J Phys Chem B* 111:7812–7824.
4. Monticelli L, et al. (2008) The MARTINI coarse-grained force field: Extension to proteins. *J Chem Theory Comput* 4:819–834.
5. Baron R, de Vries AH, Hünenberger PH, van Gunsteren WF (2006) Comparison of atomic-level and coarse-grained models for liquid hydrocarbons from molecular dynamics configurational entropy estimates. *J Phys Chem B* 110:8464–8473.
6. Berendsen HJC, Postma JPM, van Gunsteren WF, DiNola A, Haak JR (1981) Molecular dynamics with coupling to an external bath. *J Chem Phys* 81:3684–3690.
7. Steinbacher S, Bass R, Strop P, Rees DC (2007) Structures of the prokaryotic mechanosensitive channels MscL and MscS. *Curr Top Membr* 58:1–24.
8. Ollila OHS, et al. (2009) 3D pressure field in lipid membranes and membrane-protein complexes. *Phys Rev Lett* 102:078101.
9. Rowlinson JS, Widom B (1982) *Molecular Theory of Capillarity* (Clarendon, Oxford).
10. Kralchevsky PA, Nagayama K (2001) *Particles at Fluid Interfaces and Membranes* (Elsevier, Amsterdam).
11. Rawicz W, Smith BA, McIntosh TJ, Simon SA, Evans E (2008) Elasticity, strength, and water permeability of bilayers that contain raft microdomain-forming lipids. *Biophys J* 94:4725–4736.
12. Sukharev SI, Betanzos M, Chiang C-S, Guy HR (2001) The gating mechanism of the large mechanosensitive channel MscL. *Nature* 409:720–724.
13. Betanzos M, Chiang C-S, Guy HR, Sukharev, S (2002) A large iris-like expansion of a mechanosensitive channel protein induced by membrane tension. *Nat Struct Biol* 9:704–710.
14. Yefimov S, van der Giessen E, Onck PR, Marrink SJ (2008) Mechano-sensitive membrane channels in action. *Biophys J* 94:2994–3002.
15. Perozo E, Cortes DM, Sompornpisut P, Kloda A, Martinac B (2002) Open channel structure of MscL and the gating mechanism of mechanosensitive channels. *Nature* 418:942–948.
16. Anishkin A, et al. (2003) On the conformation of the COOH-terminal domain of the large mechanosensitive channel MscL. *J Gen Physiol* 121:227–244.
17. Ajouz B, Berrier C, Besnard M, Martinac B, Ghazi A (2000) Contributions of the different extramembranous domains of the mechanosensitive ion channel MscL to its response to membrane tension. *J Biol Chem* 275:1015–1022.
18. Jeon J, Voth GA (2008) Gating of the mechanosensitive channel protein MscL: The interplay of membrane and protein. *Biophys J* 94:3497–3511.
19. Elmore DE, Dougherty DA (2001) Molecular dynamics simulations of wild-type and mutant forms of the Mycobacterium tuberculosis MscL channel. *Biophys J* 81:1345–1359.
20. Maurer JA, et al. (2008) Confirming the revised C-terminal domain of the MscL crystal structure. *Biophys J* 94:4662–4667.
21. Moe PC, Levi G, Blount P (2000) Correlating a protein structure with function of a bacterial mechanosensitive channel. *J Biol Chem* 275:31121–31127.
22. Killian JA, et al. (1996) Induction of nonbilayer structures in diacylphosphatidylcholine model membranes by transmembrane α-helical peptides: Importance of hydrophobic mismatch and proposed role of tryptophans. *Biochemistry* 35:1037–1045.
23. Häse CC, le Dain AC, Martinac B (1997) Molecular dissection of the large mechanosensitive ion channel (MscL) of *E. coli*: Mutants with altered channel gating and pressure sensitivity. *J Membrane Biol* 157:17–25.
24. Blount P, Sukharev SI, Schroeder MJ, Nagle SK, Kung C (1996) Single residue substitutions that change the gating properties of a mechanosensitive channel in *Escherichia coli*. *Proc Natl Acad Sci USA* 93:11652–11657.

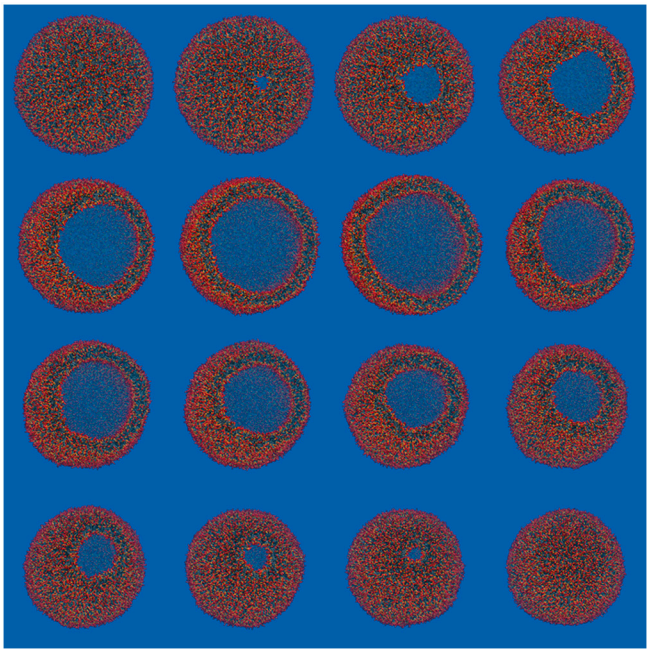

Fig. S1. Time-evolution of a membrane pore in a lipid vesicle. After nucleation the pore grows rapidly until it encompasses almost the entire width of the liposome. This is followed by a slower shrinking of the pore until full closure is reached after approximately 0.5 μs.

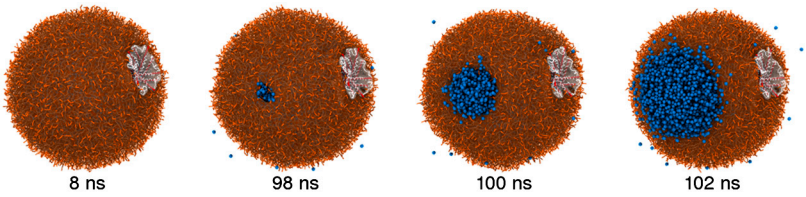

Fig. S2. Formation of a membrane pore in the presence of MscL after using a too-fast tension-loading rate. Quicker loading increases the probability of pore formation prior to MscL activation.

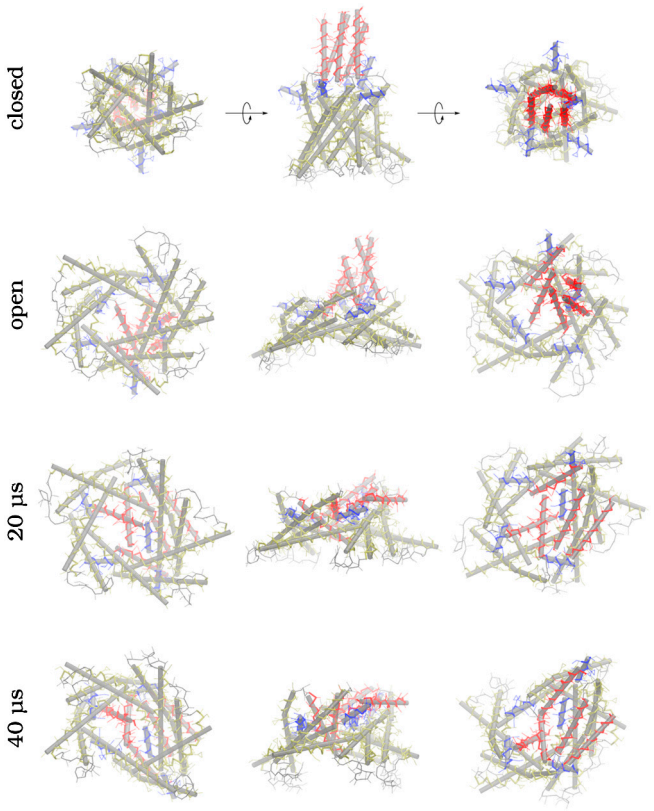

Fig. S3. Asymmetric opening of MscL in a DOPC liposome. Helical segments shown as gray cylinders with red, green, and blue backbone traces for C-terminal, transmembrane (TM1 and TM2), and S1 helices, respectively. Flattening of the surrounding lipid membrane forces the protein to change its conformation manifested by the pronounced change in the tilt angle of the transmembrane helices.

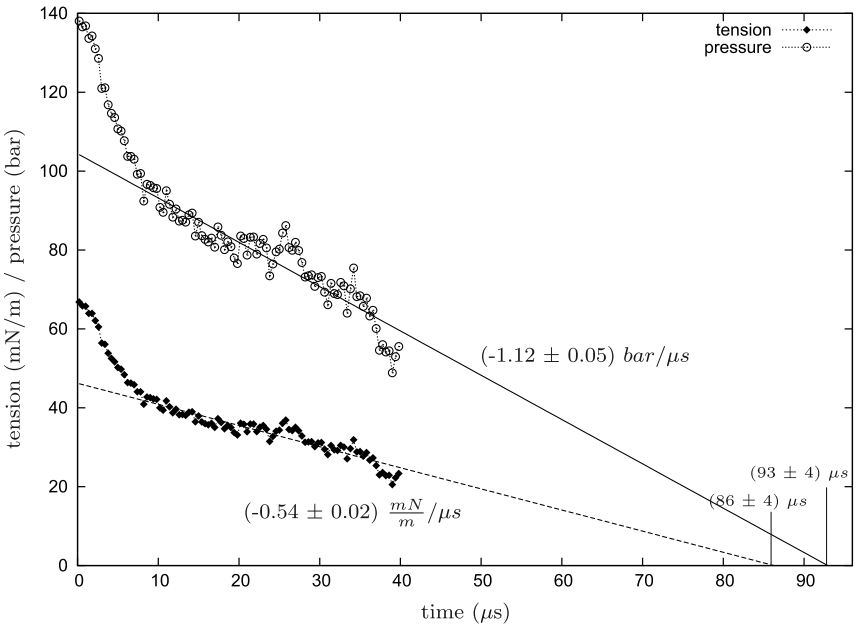

Fig. S4. Tension and pressure relaxation in a DOPC-vesicle with an active MscL. Best fitting linear decay functions shown as straight lines with estimated decay rates and mean times to reach zero level.

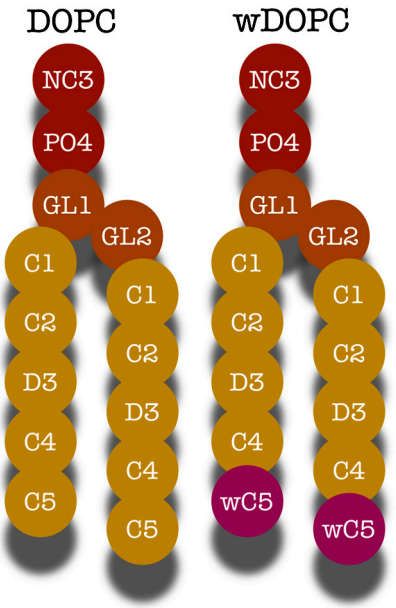

Fig. S5. MARTINI bead type definitions of both a normal (DOPC) and a water-repellent (wDOPC) dioleoyl-phosphatidylcholine.

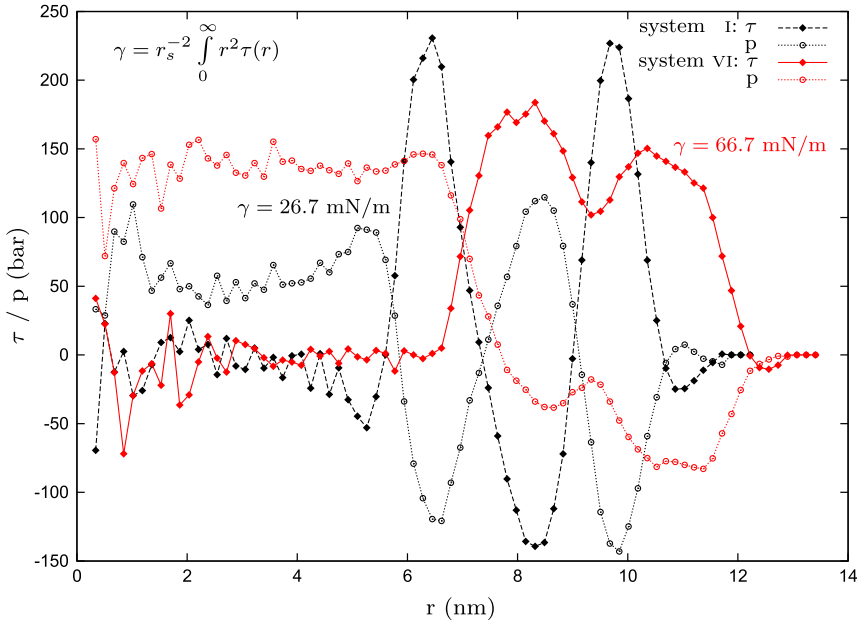

Fig. S6. Pressure differential τ and hydrostatic pressure p as a function of the distance r from the center-of-mass of the liposome in systems I and VI. The indicated values of surface tension γ are obtained from Eq. **S5** assuming an equimolar surface of tension r_s.

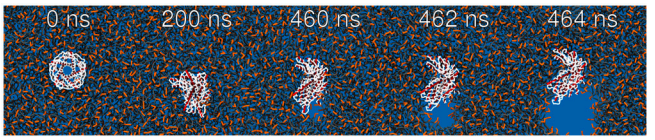

Fig. S7. Polyalanine channel facilitates the formation of a membrane pore in a stressed membrane.

Table S1. Simulated DOPC-vesicle systems

n	Lipids	Water	Time [μs]	Radius [nm]	Δ*P* [bar]	γ [mN/m]
o	2108	60093	0.4	8.08 ± 0.01	−16.6 ± 0.2	−6.7 ± 0.1
I	″	62235	1.2	8.38 ± 0.03	55.5 ± 1.0	23.3 ± 0.4
II		64377	4.0	8.68 ± 0.01	87.3 ± 0.7	37.9 ± 0.3
III		66519	4.0	8.96 ± 0.01	93.0 ± 0.6	41.6 ± 0.3
IV		68661	4.0	9.21 ± 0.01	120.6 ± 0.6	55.5 ± 0.3
V		70803	4.0	9.46 ± 0.01	117.8 ± 0.3	55.8 ± 0.2
→ VI		72945	40.0	9.68 ± 0.05	138.0 ± 1.3	66.8 ± 0.7

The first entry (system o) corresponds to the initial structure obtained by embedding a closed MscL into the spontaneously formed vesicle, and each subsequent entry corresponds to a simulation started from the final, refilled structure after *n*th pumping cycle. The total steady-state simulation times are reported excluding any preceding pumping cycles. The radius, pressure difference (Δ*P*), and tension are averages over the whole simulation time except in the last entry (system VI), which had an open channel, where only the initial 400 ns were used.

Table S2. The effect of adding water-repellent lipid tails (wDOPC) on the area per lipid and the bilayer thickness compared to a standard DOPC membrane

T	Lipid	Area/lipid [Å^2]	Thickness [nm]
290 K	DOPC	66.3 ± 0.4	4.58 ± 0.03
	wDOPC	66.2 ± 0.4	4.58 ± 0.03
300 K	DOPC	67.4 ± 0.3	4.54 ± 0.03
	wDOPC	67.2 ± 0.4	4.56 ± 0.03
310 K	DOPC	68.5 ± 0.2	4.52 ± 0.03
	wDOPC	68.4 ± 0.3	4.52 ± 0.03
323 K	DOPC	70.1 ± 0.3	4.47 ± 0.03
	wDOPC	70.0 ± 0.3	4.48 ± 0.04

Table S3. Activation likelihoods

Variant	Activation likelihood (%)
WT	37.5
V21D	100.0
Δ103	37.5
Δ12-Δ47/68-Δ101	75.0
Polyalanine	0.0
WALP	0.0

Wild-type Tb-MscL, gain-of-function mutant V21D, deletion mutants Δ103 and Δ12-Δ47/68-Δ101, and polyalanine and WALP peptide sequence replacements of TM1 and TM2 in DOPC membrane under 65 mN/m tension. Values based on eight independent 480 ns simulations for each variant.